Available online at www.sciencedirect.com
ScienceDirect
Journal of Power Sources 161 (2006) 1314–1318
JOURNAL OF POWER SOURCES
www.elsevier.com/locate/jpowsour

Short communication

Hydrothermal synthesis of nano-sized anatase TiO_2 powders for lithium secondary anode materials

Sung Woo Oh, Sang-Ho Park, Yang-Kook Sun *

Department of Chemical Engineering, Center for Information and Communication Materials, Hanyang University, Seungdong-Gu, Seoul 133-791, Republic of Korea

Received 6 March 2006; accepted 29 May 2006
Available online 28 July 2006

Abstract

Nano-sized TiO_2 powders were prepared by a hydrothermal synthetic method for use as anode materials in lithium secondary batteries. The prepared TiO_2 samples were characterized by X-ray diffraction (XRD), Brunauer–Emmett–Teller (BET) analysis, transmission electron microscopy (TEM), and electrochemical tests. TiO_2 nanoparticles were obtained at sintering temperatures between 200 and 600 °C. Calcination of the powders at 500 °C results in the formation of TiO_2 nano-sized particles of 22 nm in crystal size. These deliver a reversible discharge capacity of over 170 mAh g^{-1} between 1.5 and 3.0 V with excellent capacity retention over 95% after 100 cycles. It is speculated that the nano-sized TiO_2 powders are effective candidates for lithium secondary anode materials.

Keywords: Lithium secondary batteries; Hydrothermal method; Anatase TiO_2; Anode materials; Nanoparticles; Discharge capacity

1. Introduction

Lithium-ion batteries have emerged as power sources for modern electronics because they have the highest specific energy among all types of rechargeable battery and have no memory effect. Present commercial lithium-ion batteries use $LiCoO_2$ or $LiMn_2O_4$ as positive-electrode (cathode) materials, and graphite or carbonaceous materials as negative-electrode (anode) materials [1]. The graphite electrode does, however, have some disadvantages such as an initial capacity loss structural deformation and electrical disconnection [2]. In order to avoid these drawbacks, another class of materials, namely, transition metal oxides such as WO_3, MoO_3, and TiO_2, has been evaluated [3–5]. Titanium oxide has been found to be a good candidate as a lithium-ion host, since it has a high capacity material with low cost and no toxicity. The Li uptake has been found to be 0.5 in anatase, whereas only a weak intercalation of Li has been detectable for rutile cells. Stashans et al. [6] reported lithium insertion into anatase and rutile by quantum chemical Hartree–Fock calculations. The results predicted a higher possibility of lithium intercalation in the anatase structure than that in the rutile counterpart. Natarajan et al. [3] and Huang et al. [5] examined nano-sized TiO_2 but their materials gave TiO_2 materials small reversible capacities, namely, 50 and 140 mAh g^{-1}, respectively. A number of preparation methods have been reported [7–11] for nanostructured TiO_2, such as treating TiO_2 powders in NaOH solution, and using porous alumina as a template to obtain TiO_2 nanoribbons, nanowires, and nanotubes.

In this paper, nanocrystalline TiO_2 powders was obtained by hydrothermal treatment at 120 °C. The product has a nanocrystallized anatase structure. In order to synthesize the nano-sized TiO_2 with high quality, synthetic variable of the post calcination temperature was studied.

2. Experimental

Nano-sized TiO_2 powders were prepared as follows: 110 g of 2-butoxyethanol (Sigma–Aldrich, USA), 11.345 g of titanium butoxide (Sigma–Aldrich, USA), and 16 g of acetic acid (Junsei, Japan) were used as starting materials. The materials were put in a stainless-steel autoclave with an inner volume of 500 cm^3. After sealing, the solution was stirred magnetically at 350 rpm and the autoclave was heated to 120 °C and kept at this temper-

* Corresponding author. Tel.: +82 2 2220 0524; fax: +82 2 2282 7329.
E-mail address: yksun@hanyang.ac.kr (Y.-K. Sun).

0378-7753/$ – see front matter © 2006 Elsevier B.V. All rights reserved.
doi:10.1016/j.jpowsour.2006.05.050

ature for 2.0 h. After the hydrothermal treatment, the autoclave was cooled naturally to room temperature and the resulting solution was separated by centrifugation. The prepared powders were then post-calcined to $200 \leq T \leq 600\,^{\circ}C$ at a heating rate of $1\,^{\circ}C\,min^{-1}$.

The thermal decomposition behaviour of the precursor was examined by thermo-gravimetric analysis using a Pyris 6 thermal analyzer (TGA, Perkin-Elmer, USA). Powder X-ray diffraction (XRD, Rint-2000, Rigaku, Japan) analysis using Cu Kα radiation was employed to identify the crystalline phase of the synthesized material. The particle morphologies of the as-prepared and calcined powders were examined by means of a transimission electron microscope (TEM, JEOL 2010, Japan). Galvanostatic charge–discharge cycling was performed in a 2032-type coin type cell (Hohsen Co. Ltd., Japan). For fabrication of the working electrode, TiO_2 powder was mixed with super-P carbon black as a conductive agent and polyvinylidene fluoride (PVDF) as a binder in a mass ratio of 80:10:10. The TiO_2 and super-P carbon black were first added to a solution of PVDF in *N*-methyl-2-pyrrolidone (NMP) to make a slurry with the appropriate viscosity. The slurry was then cast on to copper foil and dried at 110 °C overnight under vacuum. Lithium foil was used as the counter electrode. The electrolyte solution was 1 M $LiPF_6$ in a mixture of ethylene carbonate (EC) and diethyl carbonate (DEC) in a 1:1 volume ratio (CHEIL Industries Inc., Korea). The cell was assembled in an argon-filled dry box and tested at room temperature (30 °C). The cell was charged and discharged at a current density of $0.4\,mA\,cm^{-2}$ with cut-off voltages of 1.5 and 3.0 V (versus Li/Li^+).

3. Results and discussion

Thermo-gravimetric analysis (TGA) data and differential temperature analysis (DTA) profiles of the obtained TiO_2 precursor are given in Fig. 1. The total weight loss value is about 20% and terminates over 400 °C. The first regions of weight loss appear below 120 °C, which are due to the removal of adsorbed water. The second step of weight loss lies between 170 and 285 °C which is attributed to the expulsion of organics that are trapped inside the pores, and also to the removal of chemisorbed water. The final step of weight loss, between 320 and 420 °C, may be due to the removal of structural hydroxyls. This will increase the number of bridging oxygens and thus the monolithic nature of the gel matrix [12]. Therefore, it is expected that pure TiO_2 particles can be obtained after calcination above 400 °C.

The precursor powders were post-calcined at various temperatures for 5 h in air. The resulting XRD patterns are shown in Fig. 2. The structure of anatase TiO_2 has the tetragonal space group $I41/amd$ with Ti^{4+} ions (octahedral sites) at positions 4(a) and O^{2-} ions at positions 8(e). The octahedral sites at the 4(b) positions are vacant with respect to cations, and may accommodate cations with almost the same ionic radii as Ti^{3+} (0.67 Å) and Ti^{4+} (0.61 Å) [13]. All peaks can be indexed to anatase TiO_2, and are in good agreement with the standard spectrum (JCPDS no.: 21-1272). On increasing the heat-treatment temperature to more than 600 °C, peaks for both the anatase and rutile phases are detected. In addition, the full-width half-maximum (FWHM) of each of the peaks become smaller with increase in calcinations temperature, which is due mainly to an increase in crystallinity and crystallite sizes. The crystallite size of the particles is calculated by applying the FWHM values of the (1 0 1) main peaks in Fig. 2 to Scherrer's equation (Eq. (1)), i.e.:

$$D_c = \frac{K^*\lambda}{\theta_{1/2}\cos\theta_B} \quad (1)$$

where K^* is a constant (ca. 0.9), λ the X-ray wavelength (1.5418 Å), θ_B the Bragg angle, and $\theta_{1/2}$ the pure diffraction broadening of a peak at half-height, that is, broadening due only to the crystallite dimensions. The variation of the crystal size (D_c) of TiO_2 nanoparticles at different temperatures is given in Table 1. The data show that there is an increase in crystalline size with increase in post-calcination temperature. The larger grain size may be caused by growth of crystals. With increasing calcination temperature, the BET specific surface area (Table 1) of

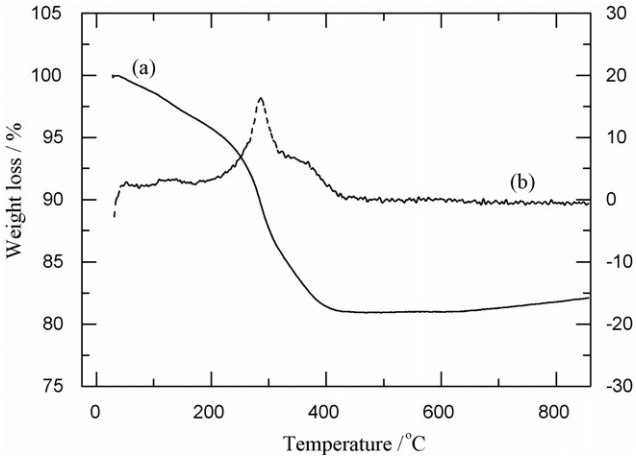

Fig. 1. (a) Thermo-gravimetric analysis (TGA) and (b) differential thermal analysis (DTA) of TiO_2 powder.

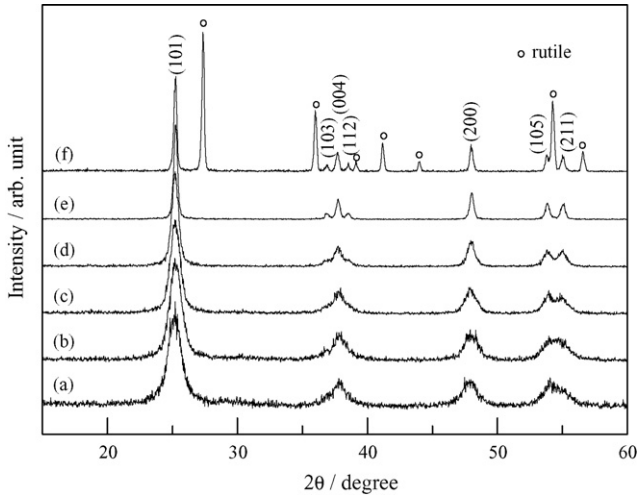

Fig. 2. X-ray diffraction patterns (XRD) for TiO_2 powders calcined at: (a) 200 °C, (b) 300 °C, (c) 400 °C, (d) 500 °C, (e) 600 °C and (f) 700 °C.

Table 1
Crystallite size and specific surface-area of TiO_2 powders prepared at various calcination temperatures

Temperature (°C)	Crystallite size (nm)	BET specific surface area ($m^2\ g^{-1}$)
200	11.2	274.6
300	12.5	195.4
400	15.2	117.2
500	22.4	60.3
600	41.1	7.25

the samples decrease. Again, this is due to the increase in grain size and particle growth during high-temperature calcination.

Transmission electron micrographs of TiO_2 powder prepared at 500 °C are presented in Fig. 3. The nanocrystalline powders are well dispersed although some agglomeration has occurred. It can be seen that TiO_2 crystals are uniform grains with an average particle size of about 20 nm, which is consistent with that calculated from the XRD data in Fig. 2(d). The diffraction ring patterns clearly show that the samples have the characteristics of nanocrystalline TiO_2.

The variation in the lattice constant of the as-prepared TiO_2 powders fired at various temperatures is shown in Fig. 4. The lattice constants were calculated by the least-squares method using the XRD data given in Fig. 2. With increasing the post-calcined temperature, the lattice constant, a decreases from 3.822(6) to 3.789(5) Å and the constant c increases from 9.847(8) to 9.533(4) Å.

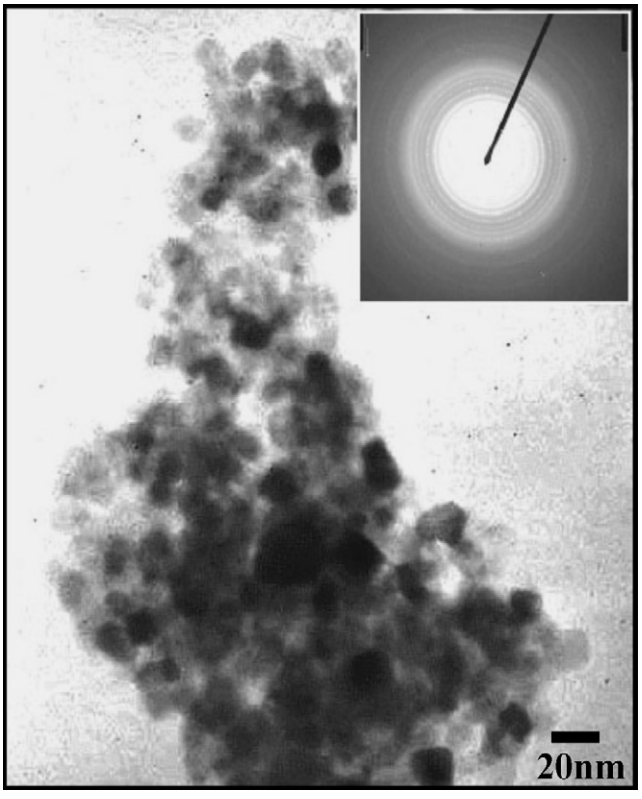

Fig. 3. Transmission electron micrograph of TiO_2 powder calcined at 500 °C; inset figure is ring pattern.

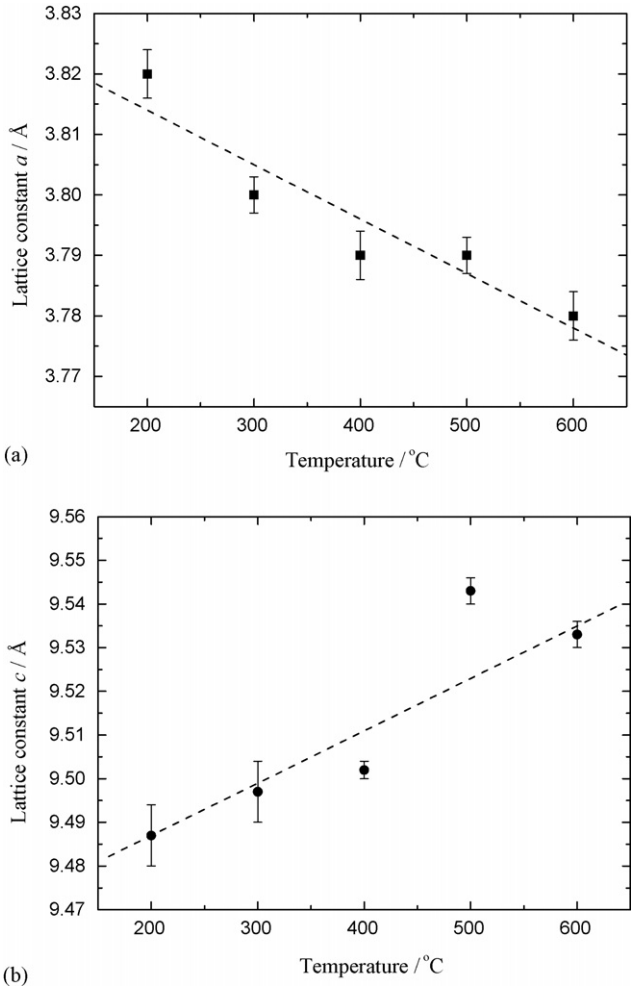

Fig. 4. (a) Lattice constants a and (b) lattice constant c of TiO_2 powders calcined at various temperatures.

Charge–discharge curves of the TiO_2 electrodes are presented in Fig. 5. The electrochemical cycling was performed over a voltage range of 1.5–3.0 V at a constant current density of 0.4 mA cm^{-2} versus a Li counter electrode. There are distinct potential plateau at/near 1.75 and 1.88 V for discharging (insertion of lithium) and charging (extraction of lithium), respectively. These are consistent with the presence of predominantly anatase as the starting material [5,6]. As cycling continues, however, the polarization ($V_{ch} - V_{dis}$) of the 500 °C samples become smaller than that of the others. This is attributed to a crystallinity of the materials. The voltage profile of the 300 °C sample displays a change at the end of discharge on the 100th cycle. Since the plateau are related to a transition between the tetragonal and orthorhombic phases with Li-intercalation into anatase TiO_2 [14], the appearance of the plateau again confirmes the formation of anatase TiO_2. Therefore, the electrochemical behaviour is assigned to the insertion/extraction of Li to/from the anatase lattice, i.e.,

$$TiO_2 + x(Li^+ + e^-) \rightarrow Li_xTiO_2 \quad (2)$$

The insertion of one Li per TiO_2 unit corresponds to a theoretical specific capacity of 335 mAh g^{-1}. The insertion coefficient, x,

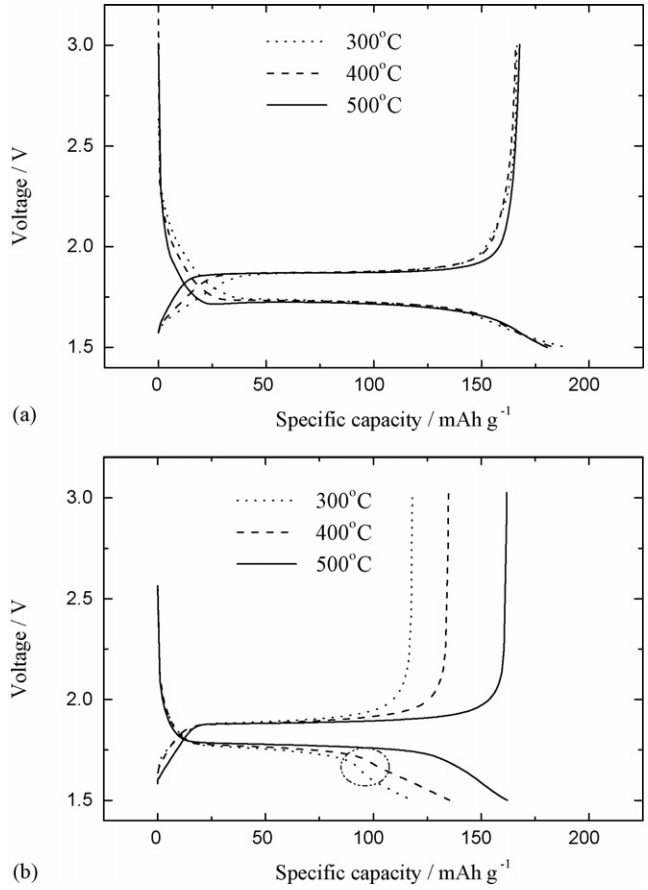

Fig. 5. Charge–discharge profiles of Li/TiO_2 cells cycled between 1.5 and 3.0 V at constant current density of 0.4 mA cm^{-2}: (a) 1st cycle; (b) 100th cycle.

in anatase is usually close to 0.5 [15]. The 500 °C sample yields a specific capacity on the first discharge of 180 mAh g^{-1}. The performance falls to 171 mAh g^{-1}. On the second cycle, i.e., capacity loss of 5%. There is, however, no appreciable change in the voltage profiles even after 100 cycles. This behaviour implies that no observable structural degradation of the nano-sized TiO_2 takes place during the lithium extraction/insertion process.

Discharge capacity versus cycle number plots at different post-calcination temperatures are given in Fig. 6. The data shows a marked capacity fading for the low-temperature samples. By contrast, the high-temperature samples suffer no capacity loss, even after 100 cycles. Poizot et al. [16] studied metal oxide systems and found that there is an optimum particle size for producing the best division of the metal particles and hence the best electrochemical properties. The work reported here shows that the electrochemical properties of TiO_2 as an anode material for lithium-ion batteries are sensitive to the particle size. Fig. 6 represents the particle size effect on the capacity retention. Despite the very small particle size (approximately 12 nm), the electrochemical reversibility of the low-temperature samples is very poor. This is attributed to instability of the crystal structure due to low crystallinity. By contrast, samples prepared over 500 °C exhibit good cycle retention, namely, almost 95% discharge capacity retention, from the 2nd to the 100th cycle. This performance is attributed to the pure TiO_2 powders that are

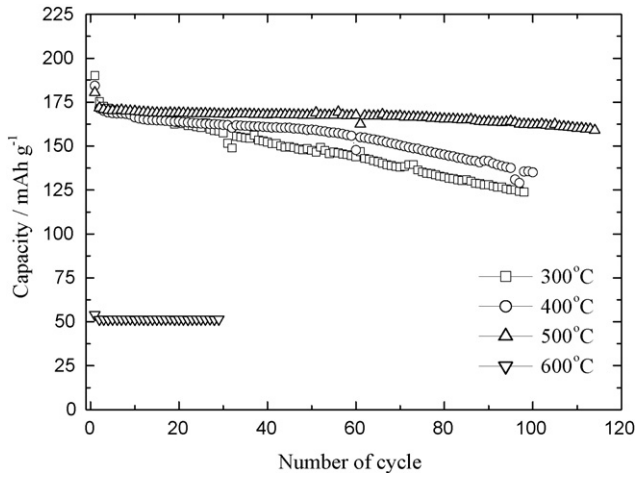

Fig. 6. Discharge capacity vs. cycle number at room temperature as a function of different sintering temperatures at a current density of 0.4 mA cm^{-2}.

obtained at a 500 °C calcination temperature, as confirmed by thermo-gravimetric analysis.

Differential capacity versus potential curves for the 1st and 100th cycle of the TiO_2 electrodes are given in Fig. 7. The

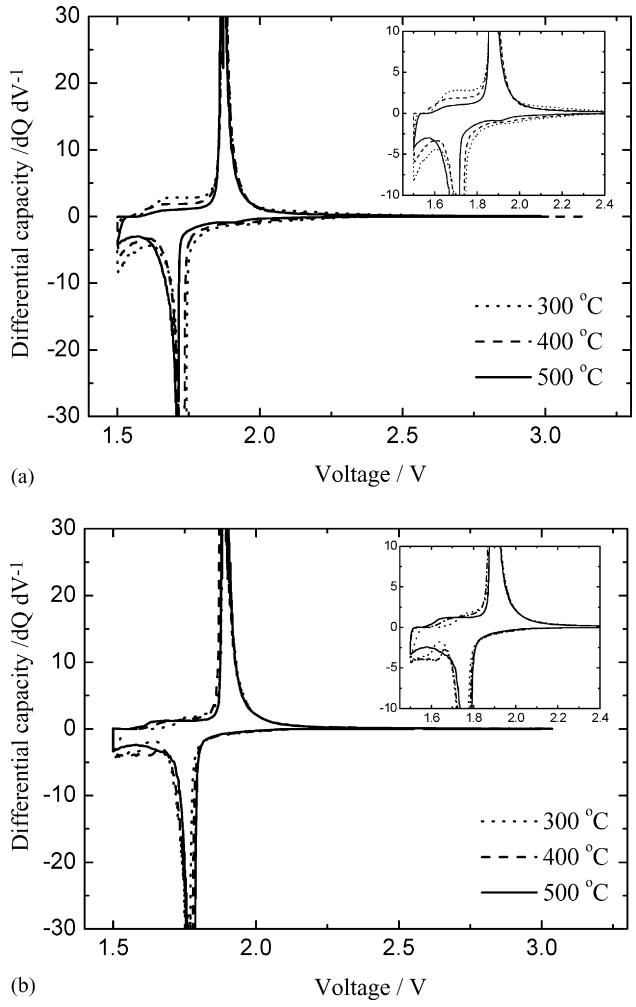

Fig. 7. Differential capacity vs. voltage for Li/TiO_2 cells: (a) 1st cycle; (b) 100th cycle.

TiO_2 electrodes show one set of reduction and oxidation peaks in the potential range of 1.5–3.0 V versus Li/Li^+. During the first discharge, a solid electrolyte interface (SEI) layer appears around the initial TiO_2 particles, and this will lead to an irreversible capacity loss. On the first cycle, a broad anodic peak is observed at about 1.87 V on charge and a sharp cathodic peak is located at 1.71 V on discharge. These two peaks suggest a one-step reversible electrochemical oxidation and reduction of TiO_2 with lithium in the electrode. The 500 °C samples do not display any difference, even on the 100th cycle, as shown in Fig. 7(b). This behaviour implies that no observable structural degradation takes place during the lithium extraction/insertion process.

4. Conclusion

A nano-sized TiO_2 powders has been successfully synthesized by hydrothermal method. The XRD patterns indicate that the powders possess the tetragonal space group $I41/amd$ of TiO_2 and TEM results of powders calcined at 500 °C show that the particles are uniform grains with an average size of approximately 20 nm. The TiO_2 powders post-calcined at 500 °C powders has a reversible capacity of 170 mAh g^{-1} with capacity retention of 95% after 100 cycles.

Acknowledgements

This work was supported by KOSEF through the Research Center for Energy Conversion and Storage.

References

[1] T. Nagaura, K. Tozawa, Prog. Batt. Solar Cells 9 (1990) 209.
[2] K.M. Abrham, Electrochim. Acta 38 (1993) 1233.
[3] C. Natarajan, K. Setoguchi, G. Nogami, Electrochim. Acta 43 (1998) 3371.
[4] J.J. Auborn, Y.L. Barbero, J. Electrochem. Soc. 134 (1987) 368.
[5] S.Y. Huang, L. Kavan, I. Exnar, M. Gratzel, J. Electrochem. Soc. 142 (1995) L142.
[6] A. Stashans, S. Lunell, R. Bergstrom, A. Hagfeldt, S.E. Lindquist, Phys. Rev. B 53 (1996) 159.
[7] Z.Y. Yuan, J.F. Colomer, B.L. Su, Chem. Phys. Lett. 363 (2002) 362.
[8] X.Y. Zhang, B.D. Yao, L.X. Zhao, C.H. Liang, L.D. Zhang, Y.Q. Mao, J. Electrochem. Soc. 148 (2001) G398.
[9] T. Kasuga, M. Hiramatsu, A. Hoson, T. Sekino, K. Niihara, Langmuir 14 (1998) 3160.
[10] H. Imai, Y. Takei, K. Shimizu, M. Matsuda, H.J. Hirashima, J. Mater. Chem. 9 (1999) 2971.
[11] T. Kasuga, M. Hiramatsu, A. Hoson, T. Sekino, K. Niihara, Adv. Mater. 11 (1999) 1307.
[12] C.P. Sibu, S. Rajesh Kumar, P. Mukundan, K.G.K. Warrier, Chem. Mater. 14 (2002) 2876.
[13] T. Ohzuku, T. Kodama, J. Power Sources 14 (1985) 153.
[14] R. Van de Krol, A. Goossens, E.A. Meulkenkamp, J. Electrochem. Soc. 146 (1990) 3150.
[15] L. Kavan, M. Gratzel, J. Rathousky, A. Zukal, J. Electrochem. Soc. 143 (1996) 394.
[16] P. Poizot, S. Laruelle, S. Grugeon, L. Dupont, J.-M. Tarascon, Nature 407 (2000) 496.